

# Outer Membrane Remodeling: The Structural Dynamics and Electrostatics of Rough Lipopolysaccharide Chemotypes

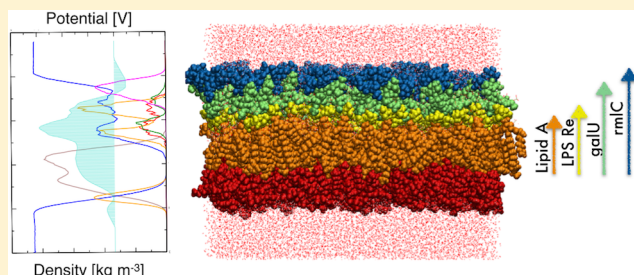
Roberta P. Dias,<sup>†</sup> Gabriel C. A. da Hora,<sup>†</sup> Madeleine Ramstedt,<sup>‡</sup> and Thereza A. Soares\*,<sup>†</sup>

<sup>†</sup>Department of Fundamental Chemistry, Federal University of Pernambuco, Cidade Universitária, Recife 50740-560, Brazil

<sup>‡</sup>Department of Chemistry, Umeå University, 90187 Umeå, Sweden

## S Supporting Information

**ABSTRACT:** Lipopolysaccharides (LPS) are the primary constituent of the outer membrane of Gram-negative bacteria such as *Pseudomonas aeruginosa*. Gram-negative bacteria can synthesize modified forms of LPS in response to environmental stimuli or due to genetic mutations, a process known as outer membrane remodeling. Chemical modifications of the LPS modulate the integrity and antibiotic susceptibility of bacterial outer membranes. It also governs microbial adhesion to tissues and artificial material surfaces. We have extended a previous model of the rough LPS to include four novel chemotypes rmlC, galU, LPS Re, and Lipid-A. Atomistic molecular dynamics (MD) simulations were performed for outer membrane models constituted of each LPS chemotypes and 1,2-dipalmitoyl-3-phosphatidylethanolamine. It is shown that the decrease in the LPS polysaccharide chain length leads to a significant increase in the diffusion coefficients for the  $\text{Ca}^{2+}$  counterions, increase in acyl chain packing (decrease in membrane fluidity), and attenuation of the negative potential across the LPS surface as positive counterions becomes more exposed to the solvent. The electrostatic potential on the LPS surfaces reflects heterogeneous charge distributions with increasingly larger patches of positive and negative potentials as the polysaccharide chain length decreases. Such a pattern originates from the spatial arrangement of charged phosphate– $\text{Ca}^{2+}$  clusters in the LPS inner-core that becomes exposed in the membrane surface as monosaccharide units are lost in the shortest chemotypes LPS Re and Lipid-A. These MD-derived conformational ensembles reproduce experimental trends and provide atom-level structural information on the rough LPS chemotypes that can help to rationalize antibiotic resistance and bacterial adhesion processes.



## 1. INTRODUCTION

Bacteria employ two-component regulatory proteins to sense environmental changes and to activate enzymes that promote chemical modifications of the bacterial outer membrane (OM).<sup>1</sup> This process, known as OM remodeling, maintains optimal membrane architecture, enhancing the bacterium ability to evade the host immune defense and colonize specific tissues.<sup>2–4</sup> It has been shown that the chemical modifications of lipopolysaccharide (LPS) molecules during OM remodeling enable bacterial resistance to cationic antimicrobial peptides.<sup>5–8</sup> These peptides permeabilize the outer membrane by disrupting the negatively charged head groups on the OM surface through displacement of divalent cations from their binding sites on LPS. The intrinsic association between chemical modifications of the LPS and bacterial resistance cationic antimicrobial peptides has been previously reported for *Pseudomonas aeruginosa*.<sup>4,9,10</sup>

Bacterial OMs are mostly composed of 1,2-dipalmitoyl-3-phosphatidylethanolamine (DPPE) in the inner leaflet and LPS in the outer leaflet.<sup>11,12</sup> Each LPS consists of a backbone containing a variable number of fatty acid chains, termed Lipid-A, covalently linked to a long polysaccharide chain.<sup>13–15</sup> The polysaccharide region is organized into a core oligosaccharide and an O-specific chain containing several identical tetrasac-

charide repeating units. These oligosaccharides, typically hexoses, determine the serotype specificity of LPS molecules whereas lipid-A is the endotoxically active part of the molecule. Upon environmental stimuli or genetic mutations, bacteria can express LPS lacking the O-specific chain and are referred to as rough LPS.<sup>16</sup> This phenotype has core oligosaccharides of varying length, which are characterized by different chemotypes depending on the sequence of decreasing length of the core sugar, e.g., Ra (complete core), Rb, Rc, Rd and Re. For almost all Gram-negative bacteria, lipid-A and the inner core components of LPS are essential whereas the O-antigen is dispensable.<sup>16,17</sup>

The experimental characterization of the structural dynamics of LPS membranes at atomic resolution is not easily attainable due to the chemical complexity of LPS molecules.<sup>18</sup> This task is made all the more difficult if one wishes to investigate membranes composed of a single LPS chemotype. We have previously developed and validated an atomistic model for LPS membranes, which relied on an improved set of specific parameters compatible with the GLYCAM and AMBER force fields.<sup>19–21</sup> This parameter set has been used to examine the

Received: January 31, 2014

Published: May 7, 2014



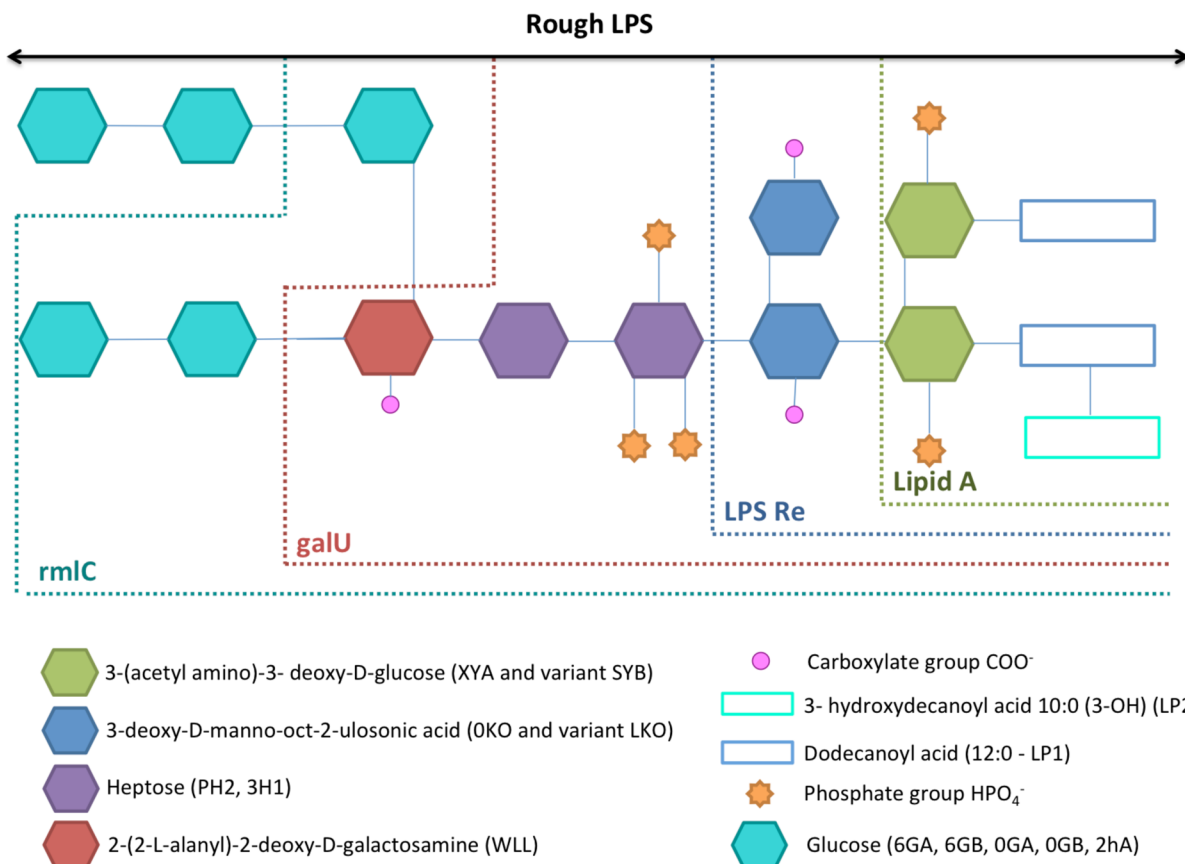


**Figure 1.** Schematic representation of the chemical structure of the rough LPS and four derived chemotypes from *P. aeruginosa*. The chemical structure and building block topologies of the rough LPS have been previously described.

**Table 1. Number of Atoms and Charged Groups in the Simulated Systems**

chemotype	number of atoms and charged groups					charge per LPS	modified <sup>a</sup> building block <sup>19</sup>
	solute	solvent	$\text{Ca}^{2+}$	$\text{HPO}_4^{2-}$	$\text{COO}^-$		
rough LPS	47 376	48 024	288	360	216	-8e	none
rmlC	44 424	48 423	288	360	216	-8e	6GAM
galU	39 888	56 193	288	360	216	-8e	WLLM
LPS Re	32 832	62 244	144	144	144	-4e	LKOM
Lipid-A	29 016	66 021	72	144	0	-2e	SYBM

<sup>a</sup>Atom type and atomic charges for modified building blocks are available in the Supporting Information.

effect of several cations on the stability of the LPS membranes and the binding mechanism of polycationic antimicrobial peptide dendrimers to LPS membranes.<sup>22,23</sup> Previous molecular dynamics (MD) simulations have also provided a detailed picture of the rough and smooth LPS chemotypes from *P. aeruginosa* with respect to structure,<sup>24–26</sup> dynamics<sup>27</sup> and free energy of ion uptake.<sup>28,29</sup> In the present work, MD simulations were used to investigate the effect of chemical remodeling on the structural dynamics and electrostatic properties of OM. The atomic parameters for the rough LPS from *P. aeruginosa* were expanded to include four new chemotypes: rmlC, galU, LPS Re and Lipid-A (Figure 1).<sup>30</sup> The abbreviations refer to mutant strains with defects in the respective genes affecting LPS core biosynthesis. Lipid-A is produced by hydrolysis of monosaccharide units.

MD simulations of bilayers composed of the respective chemotypes in the outer leaflet and DPPE in the inner leaflet showed that OM remodeling leads to significant changes in the fluidity and in the electrostatic potential on the surface of the

chemotype membranes. These atomistic models provide structural information on LPS membranes, which can complement near atomic-resolution experimental measurements and serve as a point of departure to investigate the molecular mechanisms of drug transport through the bacterial OM.

## 2. METHODOLOGY

The simulated bilayers consisted of four distinct rough LPS chemotypes, namely rmlC, galU, LPS Re and Lipid-A (Figure 1). Atomic coordinates for the initial configurations were taken from a rough LPS membrane equilibrated for 1  $\mu\text{s}$ .<sup>19</sup> Each membrane system was composed of 72 LPS molecules (outer leaflet) and 180 DPPE molecules (inner leaflet). The different LPS chemotypes were built by removing the respective monosaccharide units from the rough LPS molecule and replacing it with a hydrogen atom. The atomic charge of the added hydrogen atom was taken as the residual charge arising from removal of the monosaccharide unit. The resulting atomic charges were similar to each other and compatible with typical

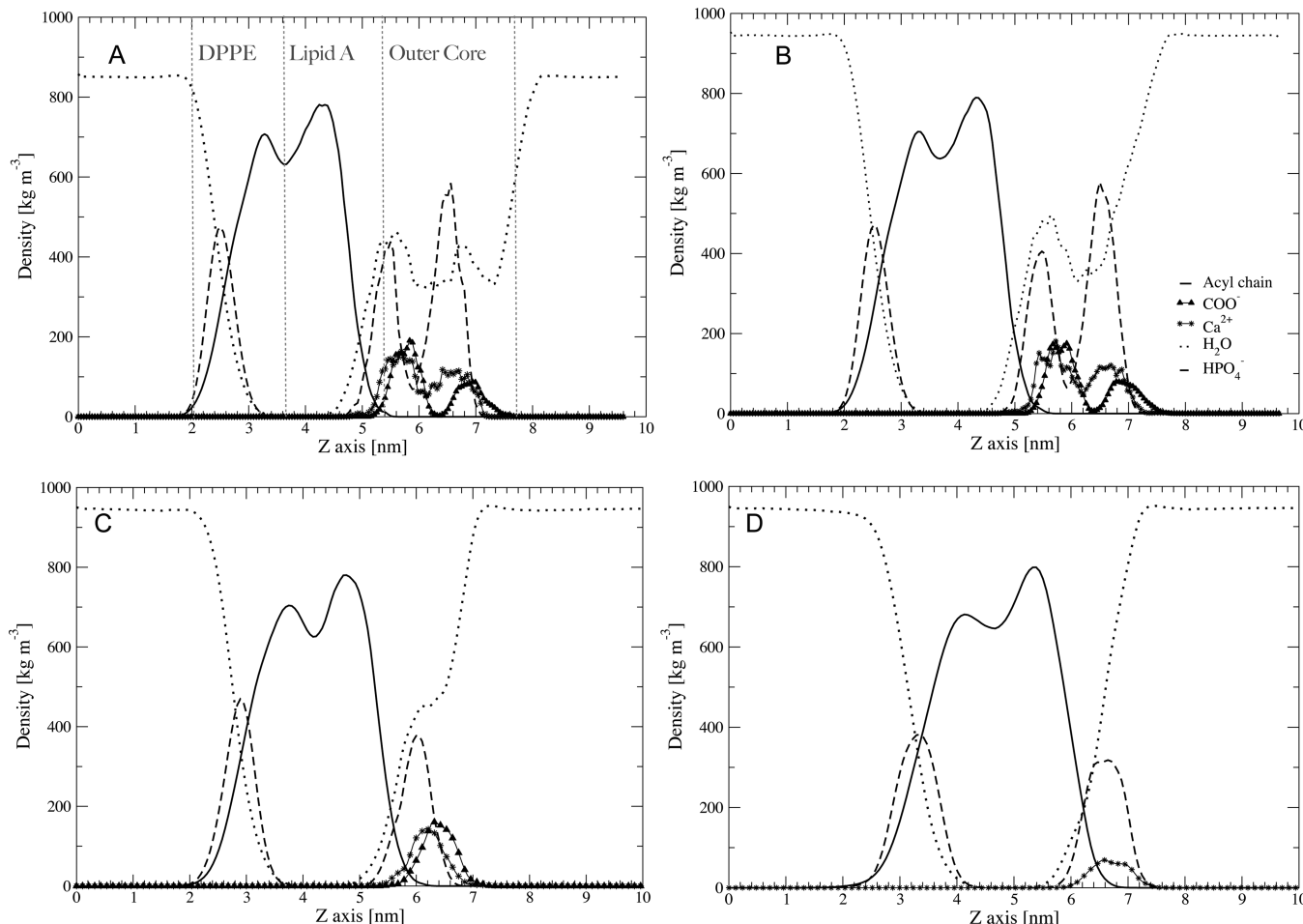


**Figure 2.** Density profiles along the axis normal to the bilayer calculated from the MD simulations of the rough LPS chemotypes rmlC (A), galU (B), LPS Re (C) and Lipid-A (D). Values were averaged over the last 20 ns.

values of capping polar hydrogens in classical force fields (about 0.4e). Atom label, types and partial atomic charges for modified building blocks are presented in the Supporting Information (Table SI-1). Counterions were added to neutralize the charged functional groups on the saccharide units at pH 7 (Table 1). A total of 288 Ca<sup>2+</sup> cations were added to the rmlC and galU LPS membranes, 144 Ca<sup>2+</sup> cations to the LPS Re membrane and 72 Ca<sup>2+</sup> cations to the Lipid-A membrane. The placement of the cations in the inner and outer core of the molecule was carried out via a multiple-step protocol previously developed for this purpose.<sup>24</sup> A brief description of the protocol is presented in the Supporting Information. The atomic parameters for the LPS and DPPE molecules have been previously published.<sup>19</sup> Periodic boundary conditions were applied to the simulations based on a rectangular box containing the fully hydrated LPS chemotype-DPPE bilayer in the *xy*-plane and normal to the *z*-axis. The TIP3P water model<sup>31</sup> was used as in our previous simulations of LPS membranes.<sup>19,24–26,32</sup> All bond lengths in the solute were kept constant using the LINCS<sup>33,34</sup> algorithm, and the water geometry was maintained with the SETTLE<sup>35</sup> algorithm. Simulations were performed in the isothermal–isobaric ensemble (NPT) with a time step of 2 fs, and in the absence of any artificial external surface tension parameter. The center of mass motion was removed at every five steps. The temperatures of the solute and solvent degrees of freedom were separately coupled to a Berendsen thermostat<sup>36</sup> at 328 K with a relaxation time of 0.4 ps. The pressure was maintained by the

weak coupling of particle coordinates and box dimensions in the *xy*-plane and along the *z*-axis separately to a pressure bath at 1.0 bar.<sup>36</sup> A semi-isotropic coordinate scaling was used with a relaxation time of 0.4 ps and a compressibility of  $4.5 \times 10^{-5}$  bar<sup>-1</sup> as appropriate for water. Bond lengths between hydrogen and heavy atoms, and the geometry of the water molecules were constrained using the linear constraint solver algorithm with a geometric tolerance of  $10^{-4}$ .<sup>33</sup> The reaction field correction and a cutoff of 1.4 nm were used for both van de Waals and long-range electrostatic interactions with a permittivity dielectric constant of 66.<sup>37–39</sup> In all cases, the pair-lists for short-range nonbonded and long-range electrostatic interactions were updated with a frequency of five timesteps. Configurations of the trajectory were recorded every 4 ps. The GROMACS package v4.0.4 was used for the MD simulations and trajectory analysis.<sup>40,41</sup> MD simulations were performed for 100 ns. The electrostatic potential across the LPS membranes was calculated by slicing the bilayers across the *xy* plane perpendicular to the *z*-axis and computing the time-averaged charge density in each slice. The electrostatic potential profile along the *z*-axis normal to the bilayer was estimated by summing this charge distribution and integrating it twice via the following equation:<sup>42</sup>

$$\psi(z) - \psi(0) = - \int_0^z dz' \int_0^{z''} \rho(z'') dz'' / \epsilon \quad (1)$$

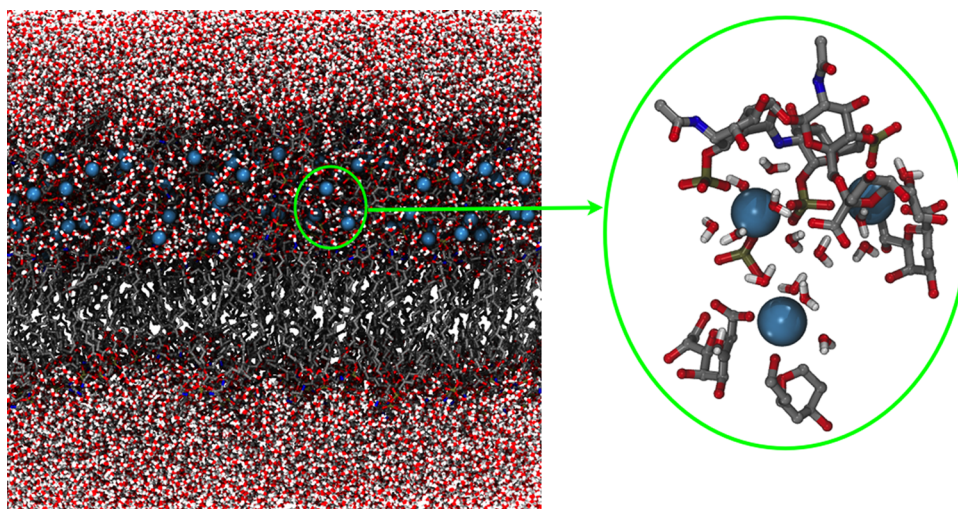


**Figure 3.** Close-up view of the functional groups involved in interactions with  $\text{Ca}^{2+}$  cations (right) in the rmlC chemotype membrane (left) of *P. aeruginosa*. On the right, only atoms within 3.5 nm from the selected  $\text{Ca}^{2+}$  atoms are shown. Hydrogen atoms are not represented for clarity.

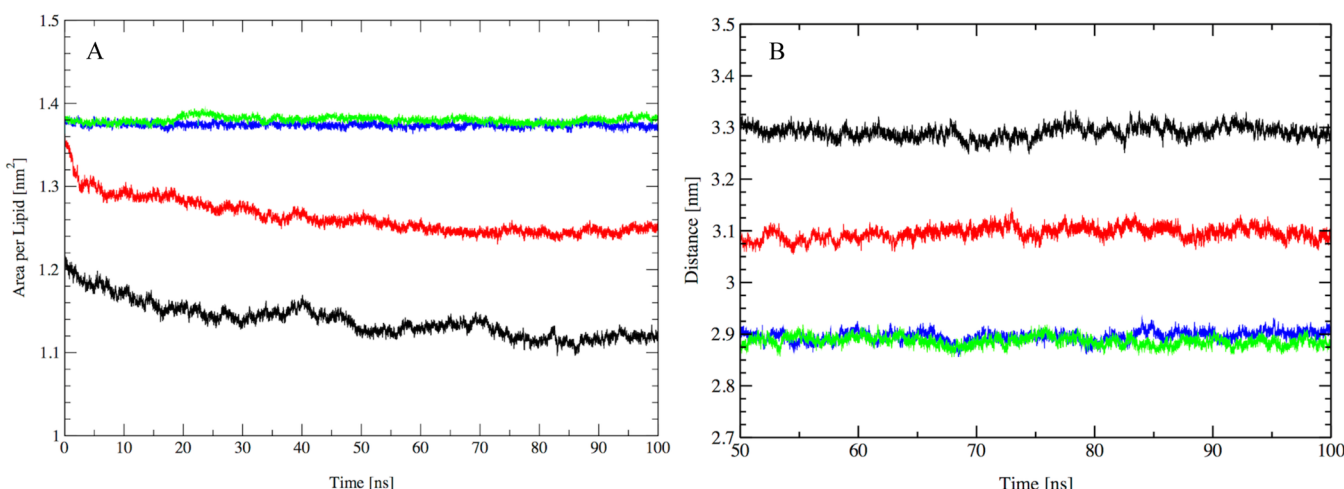


**Figure 4.** Area per lipid molecule  $A_L$  (A) and membrane thickness  $D_{\text{HH}}$  (B) from MD simulations of the rough LPS chemotypes from *P. aeruginosa*. Chemotypes are rmlC (green), galU (blue), LPS Re (red) and Lipid-A (black).

where the position  $z = 0$  is taken to be on the left side of the box. Periodic boundary conditions are not taken into account. The vacuum permittivity  $\epsilon$  is taken as 1. The electrostatic isosurface was calculated using the nonlinear Poisson–Boltzmann equation in the APBS software version 1.3.<sup>43</sup> The atomic charges and van der Waals parameters for these calculations were taken from the LPS force field used in the atomistic simulations.<sup>19</sup> The remaining data analysis procedures have been previously described.<sup>19,27</sup> Molecular visualization and figures were prepared with the VMD software version 1.9.1.<sup>44</sup>

### 3. RESULTS AND DISCUSSION

#### 3.1. Membrane Microstructure of LPS Chemotypes.

Density profiles across the axis normal to the membrane supply information on aggregate structure. The density profiles calculated from the MD simulations show the characteristic features of experimental profiles (Figure 2).<sup>45</sup> The LPS membranes maintain a lamellar arrangement with  $\text{Ca}^{2+}$  counterions distributed around the negatively charged groups. Divalent cations have been shown to stabilize LPS lamellar aggregates via cross-bridge of neighboring molecules.<sup>19,22</sup> Water molecules penetrate the LPS leaflet deep into the acyl chain

region but not the DPPE layer, which is hydrated just up to the phosphate groups. This distinctive feature of LPS membranes has been previously described by neutron scattering measurements and MD simulations.<sup>19,45</sup> Although the depth of the hydration is comparable for all four chemotype membranes, the water density profile of the rmlC system shows an increased hydration of the polysaccharide region with respect to the other chemotypes (Figure 2). Water molecules in the inner-outer core region of the rmlC membrane exhibit a structured arrangement around  $\text{Ca}^{2+}$  counterions as shown by density peaks at 5.6 and 6.4 nm along the axis normal to the membrane. These peaks fall off gradually as the polysaccharide chain length decreases, and only bulk solvent is seen in the surface of Lipid-A membrane. Structural waters are entrapped by the outer-core monosaccharides inside the LPS membrane through interactions with counterions and polysaccharide hydroxyl groups (Figure 3).

The area per lipid ( $A_L$ ) is a quantity that describes the molecular packing of a bilayer based on the interactions between its lipid constituents. It can be inferred by experimental means, providing a useful quantity for validation of molecular simulations of lipid aggregates.<sup>46</sup> In our

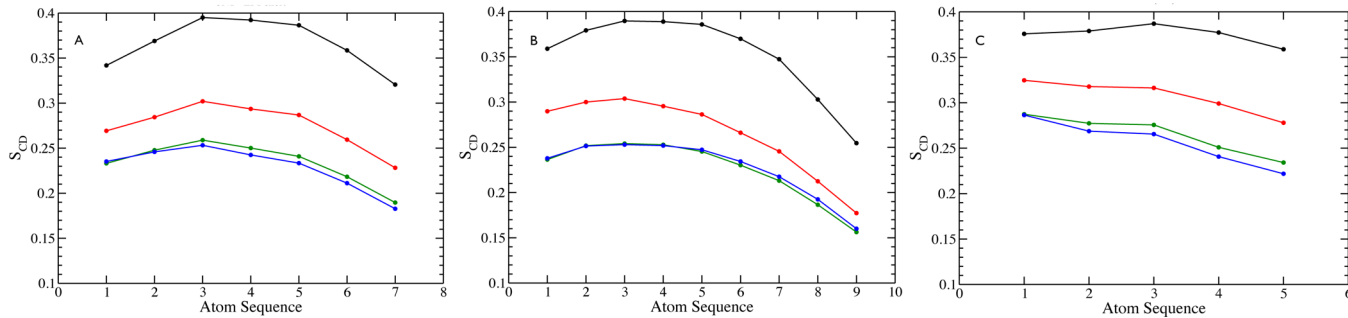


**Figure 5.** Deuterium order parameters  $S_{CD}$  calculated from MD simulations of the rough LPS chemotypes from *P. aeruginosa*.  $S_{CD}$  values are plotted as a function of the acyl segment position in the building blocks: (A) sn-1 chain (LP1), (B) sn-2 conjugated chain (LP1) and (C) sn-3 chain (LP2). Chemotypes are rmlC (green), galU (blue), LPS Re (red) and Lipid-A (black). Values were averaged over the last 20 ns.

simulations, the  $A_L$  calculated from the rmlC and galU membranes converged to ca.  $1.36 \text{ nm}^2$  (Figure 4A). Such a value is comparable to the  $A_L$  calculated from previous MD simulations of the rough LPS membrane and in agreement with experimental estimates of  $1.3 \text{ nm}^2$  for pentaacylated LPS in the liquid crystalline phase (Figure 4A).<sup>19,47</sup> The chemotypes LPS Re and Lipid-A exhibit smaller  $A_L$  and increased acyl chain packing. Our simulations show a decrease of acyl chain packing with the increase of the oligosaccharide chain length. Experimental measurements of  $A_L$  for mixed hexaacylated/heptaacylated LPS chemotypes from *Salmonella minnesota* follow the same trend.<sup>48</sup> Measured  $A_L$  values in the liquid crystalline phase vary from  $1.29 \text{ nm}^2$  for Lipid-A to  $1.39 \text{ nm}^2$  for LPS Re and  $1.42 \text{ nm}^2$  for LPS Rc (nearest analogous to the galU chemotype) and the rough LPS.<sup>48</sup> Given the pentacylated LPS structure in the simulated membranes, their corresponding  $A_L$  values are expected to be smaller than those for the hexaacylated LPS from *S. minnesota*. We remark that experimental estimates of  $A_L$  could vary significantly depending on the technique and experimental conditions used.<sup>47,48</sup> Experimental  $A_L$  values of  $1.42$  and  $1.56 \text{ nm}^2$  have been reported for the hexaacylated rough LPS from *S. minnesota* in the liquid crystalline phase. The  $A_L$  corresponding to the gel and liquid crystalline states of a given LPS chemotype can differ in values from  $0.03$  to  $0.3 \text{ nm}^2$  depending on the experimental setup.<sup>47,48</sup> Accordingly, the simulated systems rmlC, galU and LPS Re exhibit  $A_L$  consistent with the liquid crystalline state whereas the Lipid-A membrane is more compatible with the gel phase. The  $A_L$  for the rmlC and galU systems does not exhibit significant changes along the 100 ns period whereas the LPS Re and Lipid-A systems require longer convergence times, ca. 70 ns (Figure 3A). Such convergence patterns reflect the higher structural similarity of rmlC and galU to the rough LPS chemotype whose pre-equilibrated membrane coordinates were used as starting configuration for the present simulations.

The membrane (hydrophobic) thickness  $D_{HH}$  was calculated as the average distance between the center of mass of phosphate groups in the Lipid-A region of the LPS (outer leaflet) and in the DPPE headgroup (inner leaflet) (Figure 4B).  $D_{HH}$  values are inversely proportional to  $A_L$ , exhibiting a marked increase with decreasing polysaccharide length (Figure 2B). The  $D_{HH}$  increases from the longest (rmlC) to the shortest (Lipid-A) length chemotypes with a difference of  $0.4 \text{ nm}$  between the respective  $D_{HH}$  values. Previous X-ray diffraction measurements for osmotically stressed LPS multilayers indicate that phosphate interpeak distances in the Lipid-A moiety changes by  $0.5\text{--}0.55 \text{ nm}$  upon transition from gel to

liquid crystalline phases.<sup>47</sup> On the basis of experimental estimates, the calculated  $A_L$  and  $D_{HH}$  for the Lipid-A membrane are representative of an ordered liquid crystalline or gel state.<sup>47–49</sup> In fact, temperatures of the gel–liquid crystalline phase transition of LPS membranes with different sugar lengths are highest for free Lipid-A.<sup>49</sup> Because the chemotypes have been simulated at identical temperature, the experimental trend is reproduced though the absolute transition temperature  $T_c$  is not.<sup>2</sup>

**3.2. Membrane Fluidity of the LPS Chemotypes.** The degree of ordering within the lipids in the bilayer can be obtained experimentally through the determination of the carbon–deuterium order parameter  $S_{CD}$ .  $S_{CD}$  measures the relative orientation of the carbon–carbon bonds with respect to the bilayer normal. The  $S_{CD}$  of methylene groups in the dodecanoyl acid (12:0) and 3-hydroxydecanoyl acid (10:0) of the pentaacylated LPS chemotypes was calculated and compared to the available experimental data (Figure 5). The calculated deuterium parameters  $S_{CD}$  are inversely related to the area per headgroup. On that account, calculated  $S_{CD}$  values decrease from Lipid-A to LPS Re to rmlC and galU membranes (Figure 5). The  $S_{CD}$  profile along the acyl chain length in all four chemotypes follow the pattern common to saturated hydrocarbon chains with moderately low order at the beginning of the acyl chains, increasing in the middle, and decreasing at the end of the chains. The rmlC and galU chemotypes show increased fluidity compared to the shorter chemotypes LPS Re and Lipid-A. The increase in fluidity with increasing length of the sugar moiety has been previously described by experimental measurements via WAXS and FTIR spectroscopy.<sup>48</sup> Attenuated total reflectance measurements coupled to Fourier transform infrared (ATR-FTIR) spectroscopy was previously used to estimate the orientational behavior of LPS molecules from the peak position  $\chi_s$  of the symmetric stretching vibration of the methylene group around  $2850 \text{ cm}^{-1}$ .<sup>48,50–52</sup> A detailed account of the approach applied to LPS membranes is given in ref 51. Typical estimates of  $S_{CD}$  for LPS in the gel and liquid crystalline phases are  $0.70 \pm 0.05$  and  $0.25 \pm 0.05$ , respectively.<sup>51</sup> The Lipid-A from *P. aeruginosa* exhibits  $S_{CD}$  of  $0.28$  in the liquid crystalline phase.<sup>2</sup> The average  $S_{CD}$  calculated from the pentaacylated chemotypes are  $0.32$  (Lipid-A),  $0.27$  (LPS Re),  $0.24$  (galU) and  $0.23$  (rmlC) (Figure 5). These values are characteristic of liquid crystalline phase as expected under the temperature of  $328 \text{ K}$  used in the simulations. Experimental measurements indicate that the  $L\beta \rightarrow L\alpha$  transition for the LPS of *P. aeruginosa* starts at temperatures around  $303 \text{ K}$ .<sup>2,45</sup>

**Table 2. Coordination Numbers and Average Diffusion Coefficients for  $\text{Ca}^{2+}$  Ions in the Rough LPS and Chemotype Membranes**

Chemotype	$\text{Ca}^{2+}$ coordination number <sup>a</sup>					diffusion ( $10^{-9} \text{ cm}^2 \text{ s}^{-1}$ )	
	$\text{Ca}^{2+}$ -OW	$\text{Ca}^{2+}$ -P <sub>int</sub>	$\text{Ca}^{2+}$ -P <sub>ext</sub>	$\text{Ca}^{2+}$ -C <sub>int</sub>	$\text{Ca}^{2+}$ -C <sub>ext</sub>	$D_{\text{total}}$	$D_{\text{lateral}}$
rough LPS	3.75	0.62	0.89	0.62	0.02	$0.86 \pm 0.002$	$0.73 \pm 0.33$
rmlC	3.36	0.65	0.92	0.68	0.02	$0.51 \pm 1.44$	$0.56 \pm 1.08$
galU	3.73	0.65	0.91	0.68	0.07	$1.38 \pm 1.68$	$1.79 \pm 1.20$
Re	3.56	1.39		1.16		$1.66 \pm 0.18$	$1.33 \pm 0.27$
Lipid-A	4.10	2.24				$4.84 \pm 2.49$	$5.67 \pm 2.82$

<sup>a</sup>Coordination numbers correspond to the integration up to the distance of 2.8 Å in the respective radial distribution functions. Values were averaged over the final 20 ns of simulation. P<sub>int</sub> and P<sub>ext</sub> correspond to the phosphorus atom in the 3-(acetyl amino)-3-deoxy-D-glucose (SYB and XYA) and 2-(2-hydroxyethyl)-6-deoxy-D-manno-heptose (PH2) residues, respectively (see Figure 1). C<sub>int</sub> and C<sub>ext</sub> correspond to the carboxylate carbon atom in the 3-deoxy-D-manno-oct-2-ulosonic acid and 2-(2-L-alanyl)-2-deoxy-D-galactosamine residues, respectively.

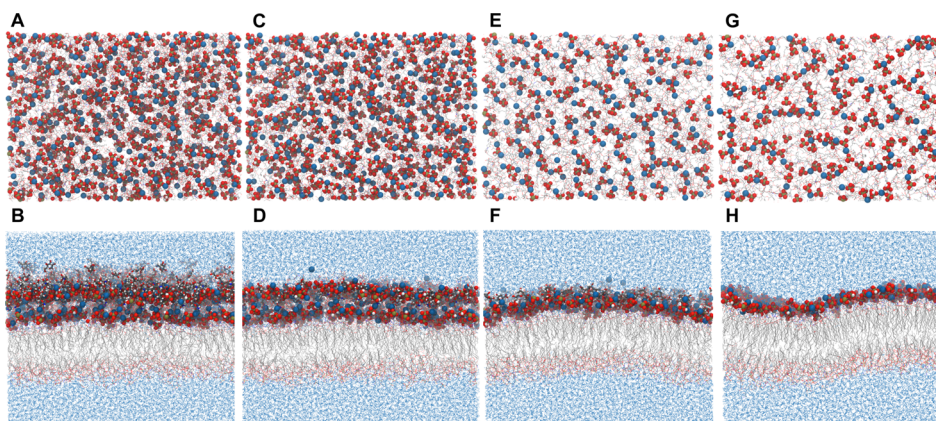


**Figure 6.** Final conformation of the LPS chemotype membranes. Views along the  $xy$ -plane (top panel) and  $z$ -axis (bottom panel) of the membrane for the rmlC (A,B), galU (C,D), LPS Re (E,F) and Lipid-A (G,H) chemotypes, respectively.  $\text{Ca}^{2+}$  ions (blue), phosphorus (gold) and oxygen (red) atoms in the LPS phosphate groups are represented by spheres. Hydrocarbon chains and selected monosaccharides are represented by sticks. Water molecules are not represented in A, C, E and G for clarity. Likewise, Only hydrogen atoms (white) from phosphate groups are represented.

**3.3. Cation Hydration and Diffusion in the LPS Chemotype Membranes.** The stability of LPS membranes is strongly influenced by electrostatic interactions between counterions and multiple phosphoryl and carboxyl substituents in the core polysaccharide region.<sup>22,53,54</sup> Cations neutralize the negative charges of these groups, which are densely packed in the LPS membrane. Previous computational simulations have shown that cations ( $\text{K}^+$ ,  $\text{Na}^+$ ,  $\text{Ba}^{2+}$ ,  $\text{Ca}^{2+}$ ,  $\text{Mg}^{2+}$ ,  $\text{Zn}^{2+}$ ) embedded in LPS membranes are highly hydrated.<sup>22</sup> It has also shown that the balance between effective membrane hydration, ionic valence and aptness to cross-link neighboring molecules modulates lamellar to nonlamellar transitions of LPS aggregates.

The  $\text{Ca}^{2+}$  ions are also hexacoordinated in all four chemotypes, as previously seen in the rough LPS membrane.<sup>19</sup> These cations bind to phosphate and carboxylate groups while remaining well hydrated (Table 2). The  $\text{Ca}^{2+}$  ions bind preferentially to the outer triphosphorylated 2-(2-hydroxyethyl)-6-deoxy-D-manno-heptose (residue PH2) followed by the phosphorylated 3-(acetyl amino)-3-deoxy-D-glucose (residues XYA and variant SYB) and carboxylated 3-deoxy-D-manno-oct-2-ulosonic acid (residues OKO and variant LKO). There is no significant binding of cations to the outer carboxylate group in the 2-(2-L-alanyl)-2-deoxy-D-galactosamine (residue WLL) (Table 2). On average, each  $\text{Ca}^{2+}$  ion is coordinated to ca. two phosphate groups and/or to one carboxylate group depending on the chemotype (Table 2). Cations in the rough LPS, rmlC and galU chemotypes are spatially distributed in two

layers around the phosphorylated carbohydrates. As the polysaccharide chain length decreases and negatively charged groups are lost, the cations become restricted to a single layer across the interface between the polysaccharide and lipid regions (Figure 6). There is only a minor increase in the number of cation-coordinated water molecules as the polysaccharide chain length decreases and  $\text{Ca}^{2+}$  ions become fully exposed to the bulk solvent as in the Lipid-A membrane. The small variation in the number of  $\text{Ca}^{2+}$ -coordinated water molecules among chemotypes is consistent with the elevated hydration of rough LPS membranes.<sup>19,22,45</sup>

Despite little changes in the hydration pattern of the LPS bound cations among different chemotypes, cations exposed to the bulk solvent exhibit higher diffusion coefficients (Table 2). This is most evident for the Lipid-A membrane where the loss of nearly all monosaccharide units places the phosphate groups and bound cations onto the membrane surface. Diffusion coefficients for  $\text{Ca}^{2+}$  ions in the Lipid-A are at least 2 times higher than in the remaining chemotypes. Hence, the overall trend is an increase in diffusion coefficients as the polysaccharide chain length decreases (Table 2). This observation suggests that the monosaccharide units and water molecules trapped within the polysaccharide region of the membrane hamper cation diffusion in the longest chemotypes. Removal of the monosaccharide units facilitates cation diffusion while simultaneously exposing  $\text{Ca}^{2+}$  binding sites onto the membrane surface.

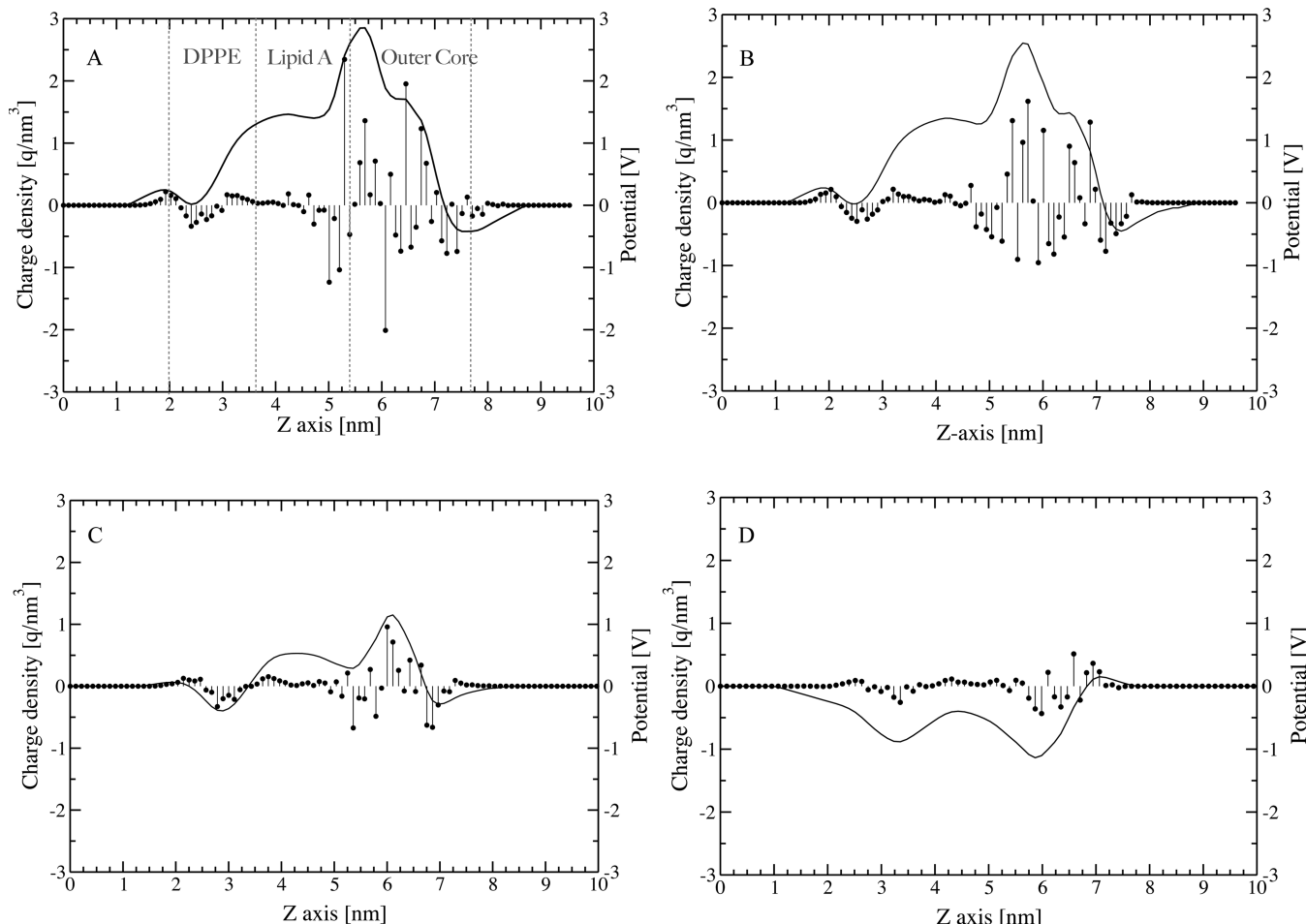


**Figure 7.** Transmembrane potential (continuous black curve) and average charge density (discrete black circle) along the axis normal to the bilayer ( $z$ -axis) calculated for the MD trajectories of the rough LPS chemotypes from *P. aeruginosa*. Chemotypes are rmlC (A), galU (B), LPS Re (C), and Lipid-A (D) chemotypes. A total of 2000 frames from the last 20 ns were used for the calculations.

**3.4. Charge Asymmetry and the Electrostatic Potential of LPS Chemotypes.** The structural arrangement of bacterial outer membrane induces a charge asymmetry across it, which plays an important role in the electrical properties of porins, low permeability and intrinsic antibiotic resistance of Gram-negative bacteria.<sup>55</sup> The structural charges associated with the membrane surface give rise to an electrostatic membrane surface potential, which will differ among the chemotypes.<sup>56</sup> MD-derived structures of LPS membranes exhibit a charge distribution whose density is highest around cation binding sites, i.e., phosphate and carboxylate groups (Figures 2 and 7). The chemical modifications of the rough LPS molecules into different chemotypes produce significant differences in the total charge per molecule (Table 2): from  $-8e$  in the rough LPS, rmlC, and galU to  $-4e$  in Re and  $-2e$  in Lipid-A (the DPPE molecule has been represented by its zwitterionic state). It is also apparent from the MD-derived structures that the charge distribution on the surface of the LPS membrane is rather heterogeneous; the more so as the polysaccharide chain length decreases (Figure 6).

The average charge density along the  $z$ -axis perpendicular to the membrane can be mapped to distinct charge groups in the LPS (right side) and DPPE (left side) molecules (Figure 7). Three main regions can be identified from the left to the right along the  $z$ -axis. In the leftmost, the first positive and negative peaks correspond to the amino and phosphate groups in the

DPPE molecule. In the center, the slightly positive charge densities correspond to the acyl chains in the LPS and DPPE molecules. The highest charge densities occur in the rightmost region of the  $z$ -axis and match the position of the phosphate and carboxylate groups in the LPS and their associated  $\text{Ca}^{2+}$  counterions (Figure 7). The DPPE surface has an average positive charge in all four chemotypes whereas the LPS surface is very negative in the galU chemotype, moderately negative in the rmlC and LPS Re chemotypes, and slightly positive in the Lipid-A chemotype. The negative charge on the LPS surface of the rmlC and LPS Re chemotypes derives from hydroxyl groups in the outermost monosaccharide units. The presence of exposed carboxylate groups on the LPS surface of the galU membrane induces a more negative surface when compared to the previous chemotypes (Figure 1). In Lipid-A, the coordination of  $\text{Ca}^{2+}$  ions to the phosphate groups on the LPS surface makes it positive (Figure 7).

Electrostatic potentials for each chemotype membrane can be calculated through the sum and consecutive integrations of the chemotype charge distribution. The electrostatic potentials for rmlC, galU, and LPS Re follow closely their respective charge distributions (Figure 7). The potential is positive on the DPPE surface and negative on the LPS surface of the bilayers with a broad positive peak in the region where the  $\text{Ca}^{2+}$  ions are located. The highest peak corresponds to cations bound deeper in the membrane and the right shoulder to cations nearer to the

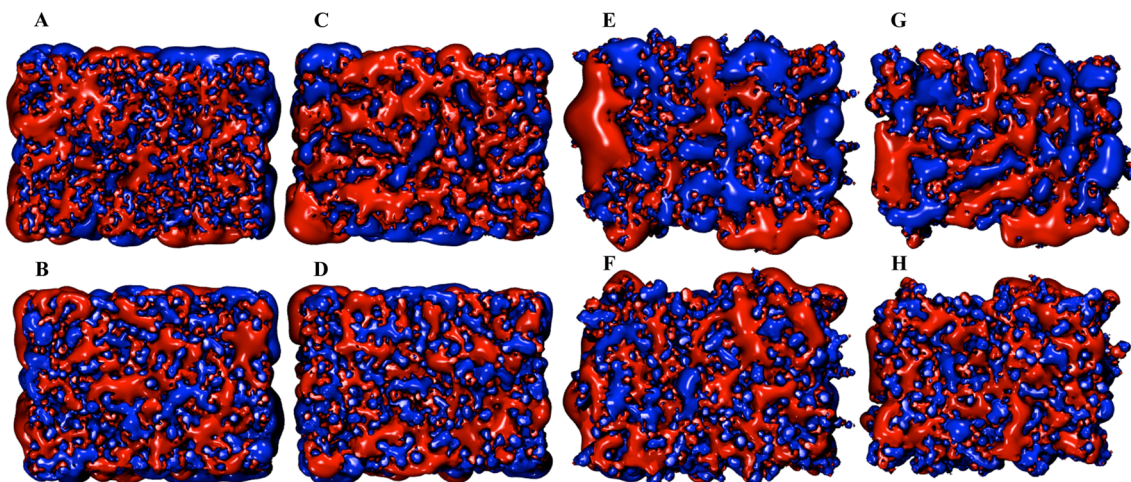


**Figure 8.** Electrostatic potential isosurfaces calculated for the final conformation of LPS chemotype membranes. Chemotypes are rmlC (A,B), galU (C,D), LPS Re (E,F) and Lipid-A (G,H). Views of the LPS (top) and DPPE (bottom) surfaces of the bilayer. The red and blue surfaces represent an equipotential contour of  $-1 \text{ } k_{\text{B}}T \text{ e}^{-1}$  and  $1 \text{ } k_{\text{B}}T \text{ e}^{-1}$ , respectively.

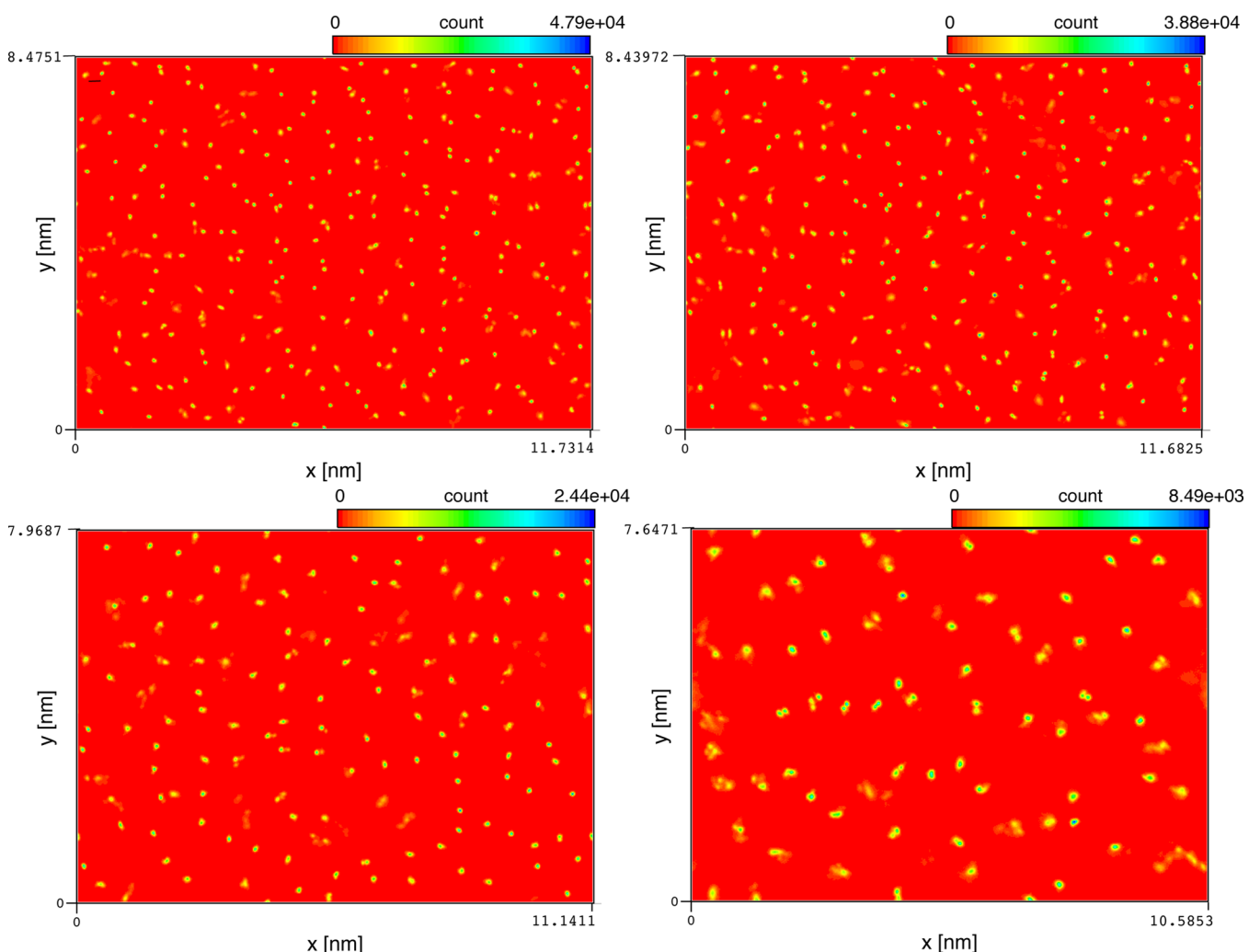


**Figure 9.** Two-dimensional number-density maps of  $\text{Ca}^{2+}$  across the LPS membrane surface averaged over 1000 frames from the last 20 ns of simulation. Chemotypes are rmlC (top-left), galU (top-right), LPS Re (bottom-left) and Lipid-A (bottom-right).

surface. In the LPS Re, this shoulder is absent as the cations are mostly confined to a single layer across the  $xy$ -plane of the membrane (Figure 6). The amplitude of this peak is lower than

in the rmlC and galU potentials due to half the number of counterions species in the LPS Re system. Conversely, the electrostatic potential is negative on the DPPE surface of the

Lipid-A membrane despite the positive charge density arising from the amino groups on this surface. The origin of the negative potential on the DPPE surface of the Lipid-A membrane is unclear. However, we hypothesize that it may result from the averaging of heterogeneously distributed charges on a surface with accentuated curvature such as the Lipid-A membrane. The decrease in the polysaccharide chain length from the rough LPS to the Lipid-A chemotype is associated with a sharp increase in the membrane curvature (Figure 6). The electrostatic potential is calculated for each trajectory frame by slicing the membrane across the *xy*-plane perpendicular to the *z*-axis of the membrane and averaging the charge density per slice. As the membrane curvature increases, charged groups become more spread over several slices with the resulting average potential containing contributions of groups located both at the membrane surface and surrounding (inner and outer) regions (Figure 6). This effect is enhanced by the unevenness of the DPPE surface in the Lipid-A membrane where a few patches of residues bulge above the rest of the surface. Therefore, three-dimensional electrostatic potentials representing the charge distribution along the membrane surfaces were obtained for the chemotype membranes (Figure 8).

A comparison of the three-dimensional electrostatic potentials for different chemotype membranes shows a similar pattern of positive–negative potentials on the respective DPPE surfaces. The three-dimensional potential across the LPS surface of the *rmlC* membrane is also reminiscent of that on the DPPE side. The LPS surface of the *galU* membrane has the most negative potential, consistent with the exposition of carboxylate groups in the membrane surface. The appearance of large positive patches on the LPS surface of the *galU* chemotype is already noticeable, and become more evident for the LPS *Re* and Lipid-A membranes (Figure 8). The latter two chemotypes exhibit a more defined isosurface pattern, particularly Lipid-A, which may reflect the spatial arrangement of charged phosphate– $\text{Ca}^{2+}$  clusters on the respective LPS surfaces (Figure 5). Such an assumption has been assessed via analysis of ion density across the chemotype membrane surfaces for the last 20 ns of simulation (Figure 9). Indeed, the ion clusters are larger and more sparse on the Lipid-A membrane compared to the remaining chemotypes. Hence, there is a gradual increase in positive regions across the LPS surface of the membranes as the polysaccharide length decreases between chemotypes. The potential on the LPS surface of the chemotypes can be estimated from the position of the outmost monosaccharide in the LPS chemotype structure as  $-428$  mV (*rmlC*),  $-618$  mV (*galU*),  $-345$  mV (LPS *Re*) and  $181$  mV (Lipid-A) (Supporting Information, Figure SI-2).

#### 4. CONCLUSIONS

We have investigated the effect of OM remodeling on the membrane structure, fluidity and surface electrostatics of rough LPS chemotypes (*rmlC*, *galU*, LPS *Re*, and Lipid-A). Toward this end, MD simulations were performed for OM models composed of a single type of LPS chemotype in the outer leaflet and DPPE molecules in the inner leaflet. Our findings can be summarized as follows: (i) on average,  $\text{Ca}^{2+}$  ions are hexa-coordinated and highly hydrated in all four chemotypes with ca. four water molecules per cation.  $\text{Ca}^{2+}$  hydration varies only slightly with changes in the length of the polysaccharide chain. Lipid-A has the most hydrated counterions; (ii) diffusion

coefficients for  $\text{Ca}^{2+}$  ions increased significantly with the decrease of the polysaccharide chain length; (iii) the acyl chain packing of the rough LPS chemotypes decreases with the increase of sugar chain length, i.e., from Lipid-A to LPS *Re*, *galU* and *rmlC*. Hence, shorter chemotypes such as Lipid-A exhibit a decrease in membrane fluidity. On average, Lipid-A has the highest values of  $S_{CD}$  consistent with the highest  $T_c$  values measured experimentally for this chemotype; (iv) the electrostatic potentials on the LPS surface of the chemotype membranes become less negative with the decrease of the polysaccharide chain length. The Lipid-A membrane has a positive potential on the LPS surface due to presence of the  $\text{Ca}^{2+}$  counterions, which form clusters with the glucosamine bound phosphates on the Lipid-A surface.

#### ■ ASSOCIATED CONTENT

##### ■ Supporting Information

The topologies, atom types and atom charges of novel building blocks. A detailed description of the protocol to generate the initial coordinates of LPS membranes as described by Soares and Straatsma<sup>24</sup> is also provided. This material is available free of charge via the Internet at <http://pubs.acs.org>.

#### ■ AUTHOR INFORMATION

##### Corresponding Author

\*Thereza A. Soares. E-mail: thereza.soares@ufpe.br.

##### Notes

The authors declare no competing financial interest.

#### ■ ACKNOWLEDGMENTS

This work was supported by the Brazilian funding agencies FACEPE, CNPq and CAPES and by the Swedish funding agency STINT. Computational resources were partially provided by the High Performance Computing Center North (HPC2N), by the Argonne Leadership Computer Facility, a scientific user facility sponsored by the U.S. Department of Energy, and the Centro Nacional de Processamento de Alto Desempenho (CENAPAD SP/MG). R.P.D. acknowledges a Junior Post-Doctoral Fellowship from CNPq.

#### ■ REFERENCES

- (1) Muller, C.; Plesiat, P.; Jeannot, K. *Antimicrob. Agents Chemother.* **2011**, *55*, 1211–1221.
- (2) Brandenburg, K.; Andra, J.; Muller, M.; Koch, M. H.; Garidel, P. *Carbohydr. Res.* **2003**, *338*, 2477–2489.
- (3) Ernst, R. K.; Guina, T.; Miller, S. I. *Microbes Infect.* **2001**, *3*, 1327–1334.
- (4) Ernst, R. K.; Yi, E. C.; Guo, L.; Lim, K. B.; Burns, J. L.; Hackett, M.; Miller, S. I. *Science* **1999**, *286*, 1561–1565.
- (5) Li, Y.; Powell, D. A.; Shaffer, S. A.; Rasko, D. A.; Pelletier, M. R.; Leszyk, J. D.; Scott, A. J.; Masoudi, A.; Goodlett, D. R.; Wang, X.; Raetz, C. R.; Ernst, R. K. *Proc. Natl. Acad. Sci. U. S. A.* **2012**, *109*, 8716–8721.
- (6) Cybulski, L. E.; Martin, M.; Mansilla, M. C.; Fernandez, A.; de Mendoza, D. *Curr. Biol.* **2010**, *20*, 1539–1544.
- (7) Rebeil, R.; Ernst, R. K.; Jarrett, C. O.; Adams, K. N.; Miller, S. I.; Hinnebusch, B. J. *J. Bacteriol.* **2006**, *188*, 1381–1388.
- (8) Delcour, A. H. *Biochim. Biophys. Acta* **2009**, *1794*, 808–816.
- (9) Fernandez, L.; Alvarez-Ortega, C.; Wiegand, I.; Olivares, J.; Kocincova, D.; Lam, J. S.; Martinez, J. L.; Hancock, R. E. *Antimicrob. Agents Chemother.* **2013**, *57*, 110–109.
- (10) Zhang, L.; Dhillon, P.; Yan, H.; Farmer, S.; Hancock, R. E. *Antimicrob. Agents Chemother.* **2000**, *44*, 3317–3321.

- (11) Lugtenberg, E. J.; Peters, R. *Biochim. Biophys. Acta* **1976**, *441*, 38–47.
- (12) Ruiz, N.; Kahne, D.; Silhavy, T. J. *Nat. Rev. Microbiol.* **2006**, *4*, 57–66.
- (13) Wilkinson, S. G. *Prog. Lipid Res.* **1996**, *35*, 283–343.
- (14) Brandenburg, K.; Wiese, A. *Curr. Top. Med. Chem.* **2004**, *4*, 1127–1146.
- (15) Erridge, C.; Bennett-Guerrero, E.; Poxton, I. R. *Microbes Infect.* **2002**, *4*, 837–851.
- (16) Raetz, C. R. H.; Whitfield, C. *Annu. Rev. Biochem.* **2002**, *71*, 635–700.
- (17) Hancock, R. E. W.; Mutharia, L. M.; Chan, L.; Darveau, R. P.; Speert, D. P.; Pier, G. B. *Infect. Immun.* **1983**, *42*, 170–177.
- (18) Wu, E. L.; Engstrom, O.; Jo, S.; Stuhlsatz, D.; Yeom, M. S.; Klauda, J. B.; Widmalm, G.; Im, W. *Biophys. J.* **2013**, *105*, 1444–1455.
- (19) Kirschner, K. N.; Lins, R. D.; Maass, A.; Soares, T. A. *J. Chem. Theory Comput.* **2012**, *28*, 4719–4731.
- (20) Kirschner, K. N.; Yongye, A. B.; Tschang, S. M.; Gonzalez-Outeirino, J.; Daniels, C. R.; Foley, B. L.; Woods, R. J. *J. Comput. Chem.* **2008**, *29*, 622–655.
- (21) Cornell, W. D.; Cieplak, P.; Bayly, C. I.; Gould, I. R.; Merz, K. M.; Ferguson, D. M.; Spellmeyer, D. C.; Fox, T.; Caldwell, J. W.; Kollman, P. A. *J. Am. Chem. Soc.* **1995**, *117*, 5179–5197.
- (22) Nascimento, A.; Pontes, F. J.; Lins, R. D.; Soares, T. A. *Chem. Commun. (Cambridge, U. K.)* **2014**, *50*, 231–233.
- (23) Ravi, H. K.; Stach, M.; Soares, T. A.; Darbre, T.; Reymond, J. L.; Casella, M. *Chem. Chem. Commun. (Cambridge, U. K.)* **2013**, *49*, 8821–8823.
- (24) Soares, T. A.; Straatsma, T. P. *Mol. Simul.* **2008**, *34*, 295–307.
- (25) Straatsma, T. P.; Soares, T. A. *Proteins: Struct., Funct., Genet.* **2009**, *74*, 475–488.
- (26) Soares, T. A.; Lins, R. D.; Straatsma, T. P. *J. Braz. Chem. Soc.* **2008**, *19*, 312–320.
- (27) Pontes, F. J. S.; Rusu, V. H.; Soares, T. A.; Lins, R. D. *J. Chem. Theory Comput.* **2012**, *8*, 3830–3838.
- (28) Lins, R. D.; Vorpagel, E. R.; Guglielmi, M.; Straatsma, T. P. *Biomacromolecules* **2008**, *9*, 29–35.
- (29) Bush, C. A.; Martin-Pastor, M.; Imbert, A. *Annu. Rev. Biophys. Biomol. Struct.* **1999**, *28*, 269–293.
- (30) Kocincova, D.; Lam, J. S. *Biochemistry (Moscow)* **2011**, *76*, 755–60.
- (31) Jorgensen, W. L.; Chandrasekhar, J.; Madura, J. D.; Impey, R. W.; Klein, M. L. *J. Chem. Phys.* **1983**, *79*, 926–936.
- (32) Lins, R. D.; Straatsma, T. P. *Biophys. J.* **2001**, *81*, 1037–1046.
- (33) Hess, B. *J. Chem. Theory Comput.* **2007**, *4*, 116–122.
- (34) Hess, B.; Bekker, H.; Berendsen, H. J. C.; Fraaije, J. G. E. M. *J. Comput. Chem.* **1997**, *18*, 1463–1472.
- (35) Miyamoto, S.; Kollman, P. A. *J. Comput. Chem.* **1992**, *13*, 952–962.
- (36) Berendsen, H. J. C.; Postma, J. P. M.; DiNola, A.; Haak, J. R. *J. Chem. Phys.* **1984**, *81*, 3684–3691.
- (37) Tironi, I. G.; Sperb, R.; Smith, P. E.; van Gunsteren, W. F. *J. Chem. Phys.* **1995**, *102*, 5451–5459.
- (38) Hochtl, P.; Boresch, S.; Bitomsky, W.; Steinhauser, O. *J. Chem. Phys.* **1998**, *109*, 4927–4937.
- (39) van der Spoel, D.; van Maaren, P. J.; Berendsen, H. J. C. *J. Chem. Phys.* **1998**, *108*, 10220–10230.
- (40) Hess, B.; Kutzner, C.; van der Spoel, D.; Lindahl, E. *J. Chem. Theory Comput.* **2008**, *4*, 435–447.
- (41) van der Spoel, D.; Lindahl, E.; Hess, B.; Groenhof, G.; Mark, A. E.; Berendsen, H. J. C. *J. Comput. Chem.* **2005**, *26*, 1701–1718.
- (42) Tieleman, D. P.; Berendsen, H. J. C. *J. Chem. Phys.* **1996**, *105*, 4871–4880.
- (43) Baker, N. A.; Sept, D.; Joseph, S.; Holst, M. J.; McCammon, J. A. *Proc. Natl. Acad. Sci. U. S. A.* **2001**, *98*, 10037–10041.
- (44) Humphrey, W.; Dalke, A.; Schulten, K. *J. Mol. Graphics* **1996**, *14*, 33–38.
- (45) Abraham, T.; Schooling, S. R.; Nieh, M. P.; Kucerka, N.; Beveridge, T. J.; Katsaras, J. *J. Phys. Chem. B* **2007**, *111*, 2477–2483.
- (46) Petrache, H. I.; Dodd, S. W.; Brown, M. F. *Biophys. J.* **2000**, *79*, 3172–3192.
- (47) Snyder, S.; Kim, D.; McIntosh, T. J. *Biochemistry* **1999**, *38*, 10758–10767.
- (48) Brandenburg, K.; Funari, S. S.; Koch, M. H.; Seydel, U. *J. Struct. Biol.* **1999**, *128*, 175–186.
- (49) Brandenburg, K.; Seydel, U. *Biochim. Biophys. Acta* **1984**, *775*, 225–238.
- (50) Brandenburg, K. *Biophys. J.* **1993**, *64*, 1215–1231.
- (51) Brandenburg, K.; Seydel, U. *Eur. J. Biochem.* **1988**, *16*, 83–94.
- (52) Brandenburg, K.; Seydel, U. *Eur. J. Biochem.* **1990**, *191*, 229–236.
- (53) Kucherka, N.; Papp-Szabo, E.; Nieh, M. P.; Harroun, T. A.; Schooling, S. R.; Pencer, J.; Nicholson, E. A.; Beveridge, T. J.; Katsaras, J. *J. Phys. Chem. B* **2008**, *112*, 8057–8062.
- (54) Langley, S.; Beveridge, T. J. *Appl. Environ. Microbiol.* **1999**, *65*, 489–498.
- (55) Nikaido, H. *Microbiol. Mol. Biol. Rev.* **2003**, *67*, 593–656.
- (56) Shephard, J.; McQuillan, A. J.; Bremer, P. J. *Appl. Environ. Microbiol.* **2008**, *74*, 6980–6986.